Bioconjugate Chemistry

Article

pubs.acs.org/bc

Graphene Oxide–Polyethylenimine Nanoconstruct as a Gene Delivery Vector and Bioimaging Tool

Hyunwoo Kim,[†] Ran Namgung,[†] Kaushik Singha,[†] Il-Kwon Oh,[‡] and Won Jong Kim*[,†]

[†]Department of Chemistry, BK School of Molecular Science, Polymer Research Institute, Pohang University of Science and Technology, Pohang 790-784, Korea

[‡]Division of Ocean Systems Engineering, School of Mechanical, Aerospace and Systems Engineering, Korea Advanced Institute of Science and Technology, Daejeon 305-701, Korea

Supporting Information

ABSTRACT: Graphene oxide (GO) has attracted an increasing amount of interest because of its potential applications in biomedical fields such as biological imaging, molecular imaging, drug/gene delivery, and cancer therapy. Moreover, GO could be fabricated by modifying its functional groups to impart specific functional or structural attributes. This study demonstrated the development of a GO-based efficient gene delivery carrier through installation of polyethylenimine, a cationic polymer, which has been widely used as a nonviral gene delivery vector. It was revealed that a hybrid gene carrier fabricated by conjugation of low-molecular weight branched polyethylenimine (BPEI) to GO increased the effective molecular weight of BPEI and consequently improved DNA binding and condensation and transfection efficiency. Furthermore, this hybrid material facilitated sensing and bioimaging because of its tunable and intrinsic electrical and optical properties. Considering the extremely high transfection efficiency comparable to that of high-molecular weight BPEI, high cell viability, and its application as a bioimaging agent, the BPEI–GO hybrid material could be extended to siRNA delivery and photothermal therapy.

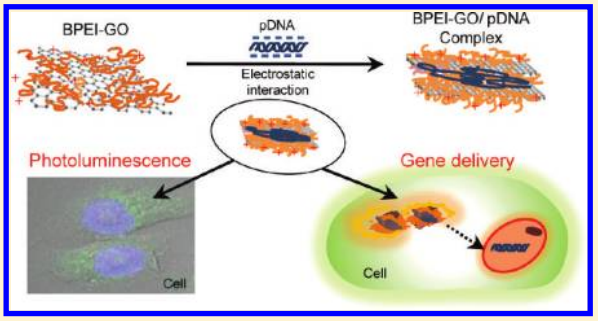

INTRODUCTION

Graphene, a single-atom-thick and two-dimensional sp^2 carbon networking material, has attracted great attention because of its remarkable electronic, mechanical, and thermal properties.[1−3] Graphene has also been used in biomedical fields, including biological sensing, molecular imaging, gene/drug delivery, and cancer therapy.[4−11] In particular, graphene oxide (GO), a precursor for graphene, is endowed with several favorable properties such as electronic, sp^2 $\pi-\pi$ interaction, and fluorescence quenching ability.[12−14] Moreover, GO possesses unique features such as facile synthesis, high water dispersibility, good colloidal stability, easily tunable surface functionalization, and good biocompatibility, which are highly conducive for bioapplications.[15] All these attributes make GO more potent than carbon nanotubes considering its in vitro and in vivo biological applications. Interestingly, sp^2 $\pi-\pi$ interaction between GO and a hydrophobic drug could facilitate the loading of the drug onto the GO surface, and this could be utilized in its facile application as a drug delivery carrier.[6,8] Similarly, the utility of GO could be extended to gene delivery and biological sensing considering the quenching properties of fluorescence-labeled DNA.[7] Strong $\pi-\pi$ stacking interaction between GO and single-stranded DNA (ssDNA) facilitates the loading of ssDNA onto GO and subsequently provides protection of DNA against enzymatic degradation.[16] However, no such interaction exists between GO and double-stranded DNA (dsDNA) as DNA bases are concealed within the double helix, preventing the generation of $\pi-\pi$ stacking interaction between dsDNA and GO.[17] Therefore, it is imperative to modify the GO to achieve effective loading of plasmid DNA (pDNA) and thereby efficient gene delivery. A feasible strategy for accomplishing such DNA complexation and transfection ability of GO could involve integration of cationic vectors.

Various viral and nonviral vector-mediated delivery strategies have been employed to achieve efficient gene transfection. The use of viral vectors, despite their high efficiency, has been impaired greatly because of the associated mutagenicity or oncogenesis, several host immune responses, and high cost of production.[18] Therefore, nonviral vectors, including cationic polymers, liposomes, dendrimers, and inorganic materials, attract significant attention in spite of their low efficacy.[19−21] There is a continuous effort to modify and refine these gene delivery systems either by adopting different strategies or by installing various functional attributes in the existing systems. Among cationic polymers such as polyethylenimine (PEI), chitosan, and Polyamidoamine (PAMAM), high molecular weight branched PEI (HMW BPEI) has been used widely as a gold standard for gene delivery vehicle. HMW BPEI showed high transfection efficiency because of enhanced cellular uptake and a high level of endosomal escape.[22,23] Nevertheless, the

Received: July 21, 2011
Revised: October 22, 2011
Published: October 31, 2011

associated cytotoxicity of HMW BPEI severely limited its use as an effective gene carrier. Interest has now shifted toward low-molecular weight (LMW) BPEI that exhibits relatively low cytotoxicity, but very poor transfection efficacy in comparison with HMW BPEI.[24,25] Furthermore, LMW BPEI exhibited enhanced cellular uptake and transfection efficiency with low cytotoxicity when it was conjugated to inorganic materials such as gold, silica, iron oxide, and carbon materials.[26−29] We presumed that hybrid gene carrier fabricated by conjugation of LMW BPEI to GO would increase the effective molecular weight of LMW BPEI and consequently improve DNA binding and condensation and transfection efficiency.

Recently, carbon-based fluorescent nanomaterials have garnered attention because of their considerably stable emissions and lower cytotoxicity, imposing less environmental concern. The photoluminescence (PL) of carbon-based nanomaterials generally emanated from isolated polyaromatic structures.[30,31] Interestingly though, GO itself contains an isolated polyaromatic structure; the PL properties of GO have not been explored much mainly because of its low emission efficiency.[32] The carboxylic and epoxy groups of GO are known to induce nonradiative recombination of localized electron−hole pairs and thereby confer the nonemissive property of GO. However, recent reports found that such nonradiative recombination of localized electron−hole pairs could be avoided by conjugating alkylamines to both the epoxy and carboxylic groups of GO through nucleophilic reaction. Consequently, the modification of nonradiative recombinative sites transforms GO into a highly efficient emitter.[33] One intention of this study has been to enhance the efficiency of PL intensity of GO by conjugating it with BPEI, and an elaborate investigation to gain further insight into the PL properties of the BPEI−GO nanoconstruct has been conducted.

We presumed that the newly designed BPEI−GO nanoconstruct may facilitate sensing and imaging because of its tunable and intrinsic electrical and optical properties. In this study, GO was modified with LMW BPEI, and their physiological properties (colloidal stability, DNA compaction ability, and transfection efficiency) and imaging properties were investigated.

EXPERIMENTAL PROCEDURES

Materials. The graphene oxide (GO) powder was obtained from Cheap-Tubes Inc. (Brattleboro, VT). Branched polyethylenimine (BPEI; molecular masses of 1.8 and 25 kDa) was purchased from Polyscience, Inc. (Warrington, PA). Triethylamine (TEA) was obtained from Samchun Chemicals. 1-Ethyl-3-[3-(dimethylamino)propyl]carbodiimide hydrochloride (EDC) was purchased from Sigma Chemical Co. (St. Louis, MO). *N*-Hydroxysuccinimide (NHS) was obtained from Fluka. The dialysis membrane (molecular mass cutoff of 3.5 kDa) was purchased from Spectrum Laboratories (Rancho Dominguez, CA). pDNA (pCMV-Luc) encoding luciferase was prepared from digestion and ligation using pGL3 (Promega, Madison, WI) and pcDNA3 (Invitrogen, Carlsbad, CA) vectors. Briefly, pGL3 was digested with XbaI and HindIII, and the following luc+ gene frame was purified by agarose gel electrophoresis and elution. Then, pCMV-Luc was constructed by insertion of the luc+ gene frame at the XbaI and HindIII restriction sites of pcDNA3 and amplified. pCMV-Luc was propagated in a chemically competent DH5α strain (GibcoBRL) and prepared from overnight bacterial cultures followed by alkaline lysis and column purification with a Qiagen plasmid Maxi kit (Qiagen, Valencia, CA). TOTO-3 iodide was purchased from Invitrogen (Eugene, OR), and mounting medium for fluorescence with DAPI was purchased from VECTOR (Burlingame, CA).

Synthesis of the BPEI−GO Conjugate. Prior to conjugation of BPEI to GO, the amount of carboxyl groups of GO was estimated by direct acid−base titration. To conjugate BPEI (M_w = 1.8 kDa) to the carboxyl groups of GO by EDC/NHS coupling, we dispersed the dried GOs in deionized water by sonication for 30 min, and EDC (54.3 mg, 0.4 mmol) and NHS (50.6 mg, 0.4 mmol) were added to the GO solution (0.5 mg/mL, 0.5 mg) in a vial. TEA (100 μL) was added to a BPEI solution (0.396 g) in deionized water. Subsequently, BPEI (M_w = 1.8 kDa) was added to the GO solution (1 mL, 0.5 mg/mL) and stirred for 1 day at room temperature. The resulting BPEI−GO solution was dialyzed against a 3500 Da molecular mass cutoff dialysis membrane in deionized water for 2 days to remove the unreacted BPEI.

Charaterization of GO and the BPEI−GO Conjugate. The concentration of BPEI in the BPEI−GO conjugate was determined by measuring the cuprammonium complex formed between BPEI and copper ion(II) at 630 nm using UV−vis spectrophotometry (UV 2550, Shimadzu), and the observed conjugation ratio of BPEI to GO was found to be 22, which is represented as BPEI−GO22. BPEI−GO5 and BPEI−GO8 were also synthesized by following the same procedure described above differing only in the amounts of BPEI1.8K used (0.04 g for BPEI−GO5 and 0.4 g for BPEI−GO8).

The size and morphology of GO and BPEI−GO were investigated with a tapping mode atomic force microscope (AFM, Nanoscope IIIa, Digital Instrument Inc.). A droplet of GO and BPEI−GO dispersion (~0.01 mg/mL) was cast onto a freshly prepared silicon oxide wafer (p-type), which was then dried at 80 °C. The chemical conjugation of BPEI to GO was confirmed by FT-IR spectroscopy (VERTEX70 FT-IR spectrophotometer, Bruker Optics) using a KBr pellet. The colloidal stability of GO, BPEI−GO, and the BPEI/GO mixture was checked by dispersing the samples in water, PBS, and DMEM medium containing 10% FBS for 30 min to 1 h at room temperature.

ζ Potential Measurements. The surface charge of GO, BPEI−GO, and BPEI−GO/pDNA complexes in DPBS buffer (pH 7.4) was confirmed by ζ potential measurements using a Zetasizer Nano Z (Malvern Instruments, Malvern, U.K.). BPEI−GO/DNA complexes were prepared at various N/P ratios [the ratio of concentrations of total nitrogen atoms (N) of BPEI to the phosphate groups (P) of pDNA] (2, 5, 10, and 20) by addition of the BPEI−GO suspension to the pDNA solution in DPBS buffer (pH 7.4). The final pDNA concentration was adjusted to 33 μg/mL. The mixtures were then incubated for 30 min prior to measurement of the ζ potential at room temperature.

Agarose Gel Retardation Assay. Complexes of pDNA with GO, BPEI1.8K, and BPEI−GO were prepared by addition of the sample suspension (10 μL) to the pDNA solution (10 μL) at various N/P ratios ranging from 0 to 50 in DPBS buffer and incubation for 30 min at room temperature. The complexes were then electrophoresed through a 1% (w/v) agarose gel containing ethidium bromide (EtBr, 0.5 μg/mL) in 0.5 TAE (Tris-acetate-EDTA) buffer at 100 V for 20 min. The gel was then analyzed on a UV illuminator (wiseUV WUV, DAIHAN Scientific, Seoul, Korea).

Cell Culture. A human cervical cancer cell line (HeLa) and a human prostate cancer cell line (PC-3) were cultured in a

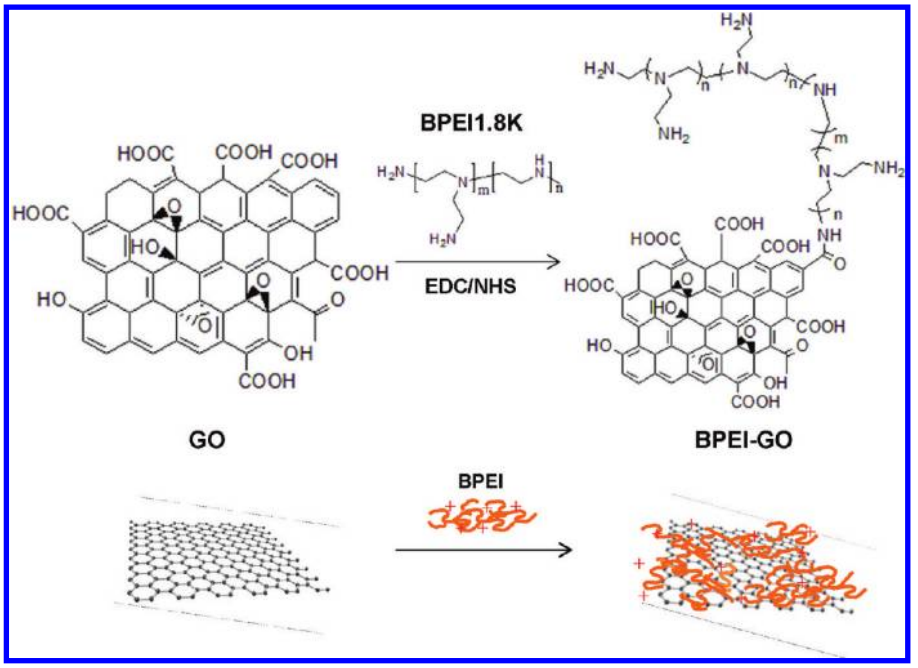

Figure 1. Synthetic scheme of BPEI−GO. BPEI (M_w = 1.8 kDa) was conjugated to the carboxyl groups of GO by EDC/NHS coupling. The dried GO was dispersed in deionized water by sonication for 30 min. EDC and NHS were added to the GO solution. TEA was added to a BPEI solution in deionized water. Subsequently, BPEI was added to the GO solution, and the mixture was stirred for 1 day at room temperature.

humidified atmosphere (5% CO_2) at 37 °C. Dulbecco's modified Eagle's medium (DMEM), Roswell Park Memorial Institute medium (RPMI-1640), penicillin/streptomycin, fetal bovine serum (FBS), and Dulbecco's phosphate-buffered saline (DPBS) were purchased from Invitrogen-Gibco (Carlsbad, CA). The luciferase assay kit and reporter lysis buffer were purchased from Promega, and the bicinchoninic acid (BCA) protein assay reagent kit was purchased from Pierce Chemical Co. (Rockford, IL). Cell viability was estimated by using 3-(4,5-dimethylthiazol-2-yl)-2,5-diphenyltetrazolium bromide (MTT) (Sigma-Aldrich).

Luciferase Reporter Gene Assay. HeLa and PC-3 cells were seeded on 24-well culture plates at an initial density of 7 × 10^4 cells/well and incubated for 24 h in 500 μL of DMEM or RPMI-1640 containing 10% FBS at 37 °C in a humidified atmosphere with 5% CO_2. Samples (10 μL) were complexed with 2 μg of pDNA (10 μL) at various N/P ratios and incubated for 30 min. The cells were incubated with the complexes (20 μL) in 250 μL of serum-free medium for 4 h and then incubated for 18 h in 500 μL of fresh medium containing 10% FBS. After the cells had been washed with DPBS, lysis buffer was then added to the well (200 μL/well) for lysis of cells. Luciferase reporter gene expression was evaluated using a microplate spectrofluorometer (VICTOR3 V Multilabel Counter, Perkin-Elmer, Wellesley, MA).

Cytotoxicity Assay. The cytotoxicity of complexes was evaluated by the MTT assay. Cells were seeded onto 96-well plates at a density of 1 × 10^4 cells/well and incubated for 24 h. pDNA (0.2 μg/μL) was complexed with the samples at various N/P ratios in DPBS buffer and incubated for 30 min. Complexes were incubated with the cells for 4 h in 100 μL of serum-free medium, followed by further incubation for 20 h in 200 μL of medium containing 10% FBS. Cell medium was replaced with 200 μL of fresh medium and 20 μL of an MTT solution (5 mg/mL) and incubated for an additional 4 h. The medium was then removed, and 150 μL of DMSO was added to the wells to dissolve the internalized purple formazan crystals. An aliquot (100 μL) was taken from each well and transferred to a fresh 96-well plate. The absorption was measured at 570 nm using a microplate spectrofluorometer. The relative percentage of the control cells (nontreated), which were not exposed to the transfection system, was used to represent 100% cell viability.

Photoluminescence Spectrum Study. The photoluminescence (PL) spectrum was recorded with a spectrofluorophotometer (RF-5301PC, SHIMADZU) to obtain the PL profile of BPEI−GO. The PL of BPEI−GO was scanned at various excitation wavelength ranging from 400 to 480 nm, and the λ_{max} excitation was found to be 480 nm. The λ_{max} excitation and λ_{max} emission of BPEI−GO were measured at 480 and 520 nm, respectively.

Confocal Fluorescence Microscopy Study. HeLa cells were seeded at a density of 1 × 10^4 cells/well in a 12-well plate over glass coverslips. Cells were incubated with BPEI−GO/pDNA complexes for a certain period of time at 37 °C. After the cellular uptake had been quenched via addition of cold DPBS, cells were washed twice with cold DPBS and fixed with 4% paraformaldehyde for 30 min at room temperature. Cells on a coverslip were mounted in Vectashield antifade mounting medium with DAPI (Vetor Laboratories), observed with a confocal laser scanning microscope (CLSM), and analyzed with Olympus Fluoview version 1.5.

■ RESULTS AND DISCUSSION

Synthesis and Characterization of BPEI−GO. To construct the GO-based gene delivery vector, LMW BPEI1.8K (M_w = 1.8 kDa) was covalently conjugated to the carboxyl group of GO using EDC/NHS chemistry (Figure 1). The amount of conjugated BPEI in BPEI−GO was analyzed by measuring the UV−vis absorbance of cuprammonium complexes of BPEI−GO at 630 nm, and the estimated conjugation ratios of BPEI to GO were found to be 5, 8, and 22 and were

dx.doi.org/10.1021/bc200397j | Bioconjugate Chem. 2011, 22, 2558−2567

denoted as BPEI−GO5, BPEI−GO8, and BPEI−GO22, respectively (Table 1). The successful conjugation of the

Table 1. Characteristics of the BPEI−GO Conjugate[a]

	reaction condition (equivalent to COOH of GO[b])			BPEI in BPEI−GO[c]		
BPEI−GO	BPEI (equiv)	EDC/NHS (equiv)	GO (mg)	mg	μmol	BPEI:GO conjugation ratio[d] (w/w)
BPEI−GO5	10	20		2.33	1.29	5
BPEI−GO8	10	200	0.5	3.94	2.18	8
BPEI−GO22	100	200		11.07	6.15	22

[a]The reaction was conducted in deionized water. [b]The amount of carboxyl groups of GO was estimated by direct acid−base titration. On the basis of the estimated carboxylic acid content, an excess molar ratio of EDC/NHS and BPEI were added to the GO for GO−BPEI synthesis. [c]The concentration of BPEI in BPEI−GO was determined by measuring the cuprammonium complex formed between PEI and copper(II) at 630 nm using UV−vis spectrophotometry. [d]Conjugation ratios were determined by calculating the weight of BPEI and GO in the BPEI−GO conjugate.

carboxyl group of GO and amino group of BPEI was confirmed by FT-IR spectroscopy, which showed the characteristic peak of the amide bond at 1630−1695 cm^{-1}, confirming the reported value (Figure 2). The appearance of the vibration band around

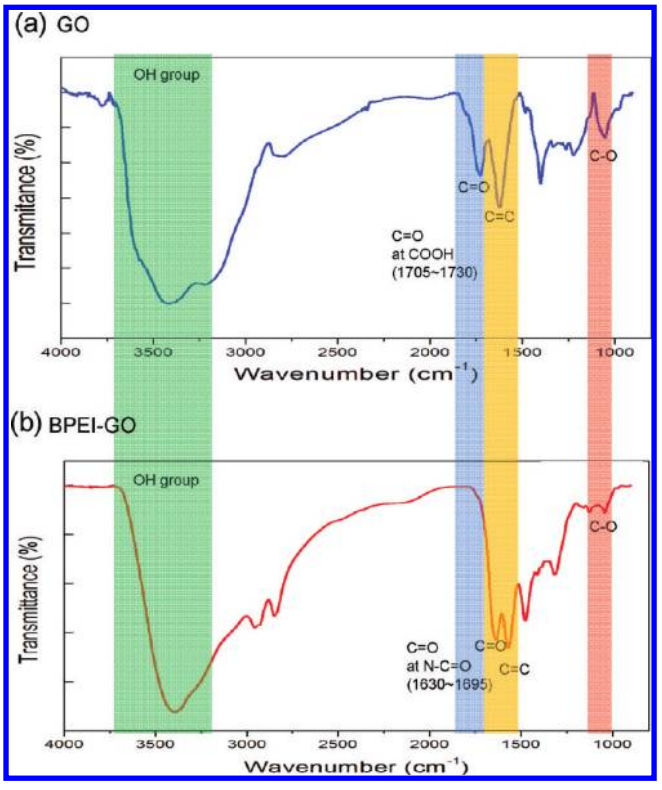

Figure 2. FT-IR spectra of GO (a) and BPEI−GO (b). Conjugation of the carboxyl group of GO and the amino group of BPEI was confirmed by FT-IR spectroscopy, which showed the characteristic peak of the amide bond at 1630−1695 cm^{-1}.

1650 cm^{-1} due to the C═O stretching of the primary amide in BPEI−GO and the disappearance of the carboxylic group bands at 1733 cm^{-1} of pristine GO substantiated the formation of amide linkages. Furthermore, in the case of BPEI−GO, the absence of the band at 1050 cm^{-1} that was observed earlier in GO due to the presence of epoxide moieties clearly established the successful chemical conjugation. However, the band at 1626 cm^{-1} arising due to the C═C vibration of aromatic rings was observed in both GO and BPEI−GO and implied the preservation of the sp^2 character in BPEI−GO after the chemical conjugation.[34,35]

Colloidal property constitutes an important parameter in evaluating the viability of a biomaterial in a biological application. Accordingly, colloidal stability of GO, the BPEI/GO mixture, and the BPEI−GO conjugate was investigated in water, PBS, and 10% serum-containing medium (Figure 3).

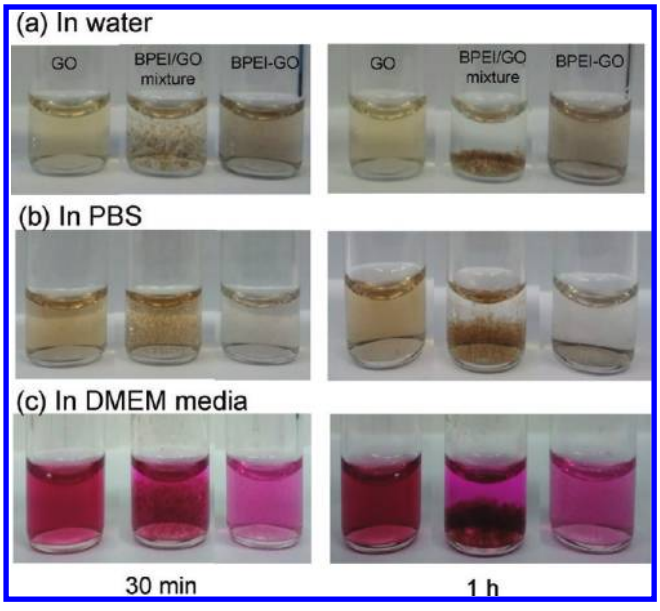

Figure 3. Colloidal stability of GO, the BPEI/GO mixture, and BPEI−GO22 in water (a), PBS (b), and DMEM medium containing 10% FBS (c).

Noticeable aggregation was observed for the BPEI/GO mixture, while no aggregation was observed for unmodified GO or the chemically modified BPEI−GO22 conjugate even after longer incubation times in all types of media under investigation. Such observations could easily be explained considering the charge repulsion phenomenon of colloids. In general, identical charges repel each other to provide colloidal stability. Therefore, negatively charged GO remains in good colloidal stability in solution because of the charge repulsion of GO particles (Figure S2 of the Supporting Information). Likewise, in the case of BPEI−GO, GO was evenly and completely coated with positively charged BPEI and showed excellent colloidal stability even under physiological conditions (10% serum-containing medium). However, colloidal stability was found to be very low for a simple BPEI/GO mixture that contained two oppositely charged molecules and allowed the charge interaction leading to aggregation. The effect of surface charges on colloidal stability was also be corroborated by ζ potential measurements as described later.

The size and morphology of GO and BPEI−GO with various degrees of conjugation was studied by AFM (Figure 4). The

dx.doi.org/10.1021/bc200397j | Bioconjugate Chem. 2011, 22, 2558−2567

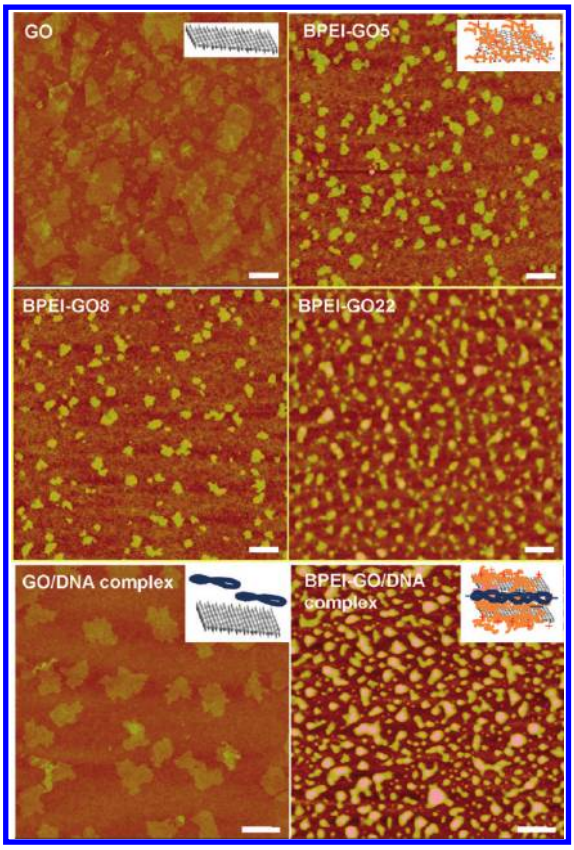

Figure 4. AFM images of GO, BPEI–GO, the GO/DNA complex, and the BPEI–GO/DNA complex. A droplet of GO and BPEI–GO dispersion was cast onto a freshly prepared silicon oxide wafer (p-type), followed by drying at 80 °C. The scale bar is 500 nm.

size of the unmodified GO was found to be 500–600 nm, and a thickness of 0.6–1.3 nm corresponds to one to two layers of GO. Interestingly, the BPEI–GO conjugate showed a reduced size of 100–200 nm and an increased thickness of 6–8 nm. However, the increase in the ratio of the degree of conjugation of BPEI to GO had little effect on the size and thickness of the BPEI–GO conjugates. Then, the effect of complexation with pDNA on the size and morphology of GO and BPEI–GO was investigated by AFM. As expected, complexation of GO with pDNA did not change the size and thickness of GO, which clearly demonstrated the absence of any significant interaction between GO and pDNA. In contrast, the size and thickness of BPEI–GO/pDNA complexes were increased to 300–400 and 16–18 nm, respectively, upon formation of the complex. The reduced size of BPEI–GO compared to that of GO could be attributed to the folding of the GO sheet. During EDC/NHS-mediated conjugation, the primary amine of BPEI not only formed an amide linkage with the carboxylic groups residing at the GO edges but also underwent a ring-opening reaction with the epoxy functionalities at the basal plane of the GO sheets.[36] It could be assumed that the free ends of the conjugated BPEI formed an amide linkage with the carboxylic groups present in the same or other GO sheet leading to the folding and cross-linking of the GO sheets, which resulted in the reduced size and increased thickness arising from the stacking of the GO sheets. The increase in the size and thickness of the BPEI–GO conjugate upon complexation with pDNA could be explained by considering the electrostatic interaction between the negatively charged pDNA and positively charged BPEI–GO conjugates. pDNA was thought to be sandwiched between two BPEI–GO stakes giving rise to the increased thickness. Such vertical stacking might lead to a multilayer structure. Similarly, complexation involving the laterally conjugated BPEI and pDNA might lead to lateral elongation and, hence, the increased size of the BPEI–GO/pDNA complex.

Formation of the Polyelectrolyte Complex and ζ Potential Measurements. It is necessary for an efficient gene carrier to interact with pDNA generally through electrostatic interaction and form a nanosized complex. As described above, unmodified GO does not interact with pDNA and, therefore, cannot form a complex with pDNA. However, GO modified with BPEI should acquire positive surface charge and is expected to interact with pDNA having a negatively charged phosphate backbone. Therefore, in this study, formation of a complex of the gene carrier with pDNA was investigated by agarose gel electrophoresis analysis. As expected, GO did not form a complex with pDNA even at higher N/P ratios of 50 because of its negative charge, while BPEI underwent complete complexation with pDNA at a low N/P ratio of 5 (Figure 5a). Although BPEI–GO5 having a lower conjugation ratio formed complexes with N/P ratios of

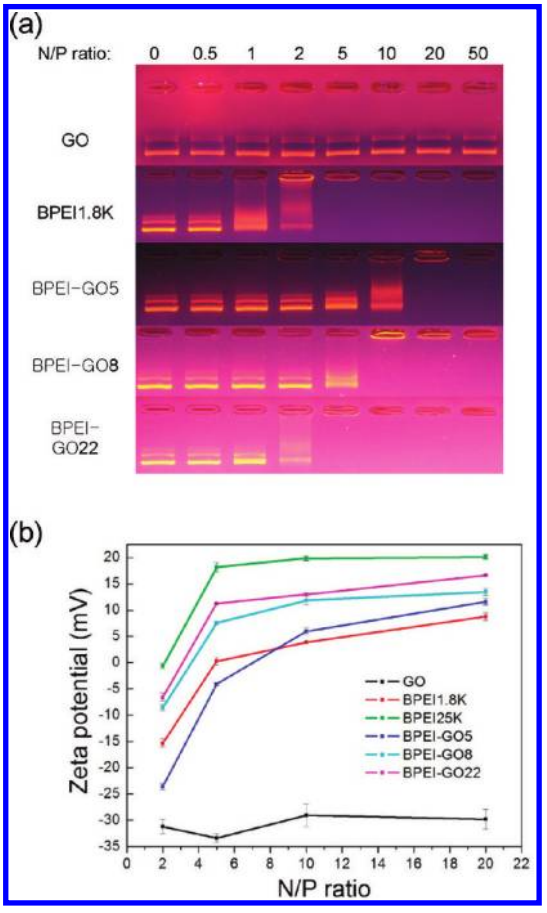

Figure 5. Agarose gel retardation study (a) and ζ potential measurements (b) of pDNA complexed with GO, BPEI1.8K, and BPEI–GO conjugates at various N/P ratios. (a) Complexes of pDNA with GO, BPEI1.8K, and BPEI–GO conjugates were electrophoresed through a 1% (w/v) agarose gel and then analyzed with a UV illuminator. (b) The final pDNA concentration for ζ potential measurement was adjusted to 33 μg/mL. The complexes were then incubated for 30 min prior to the measurement of ζ potential at room temperature.

dx.doi.org/10.1021/bc200397j | Bioconjugate Chem. 2011, 22, 2558–2567

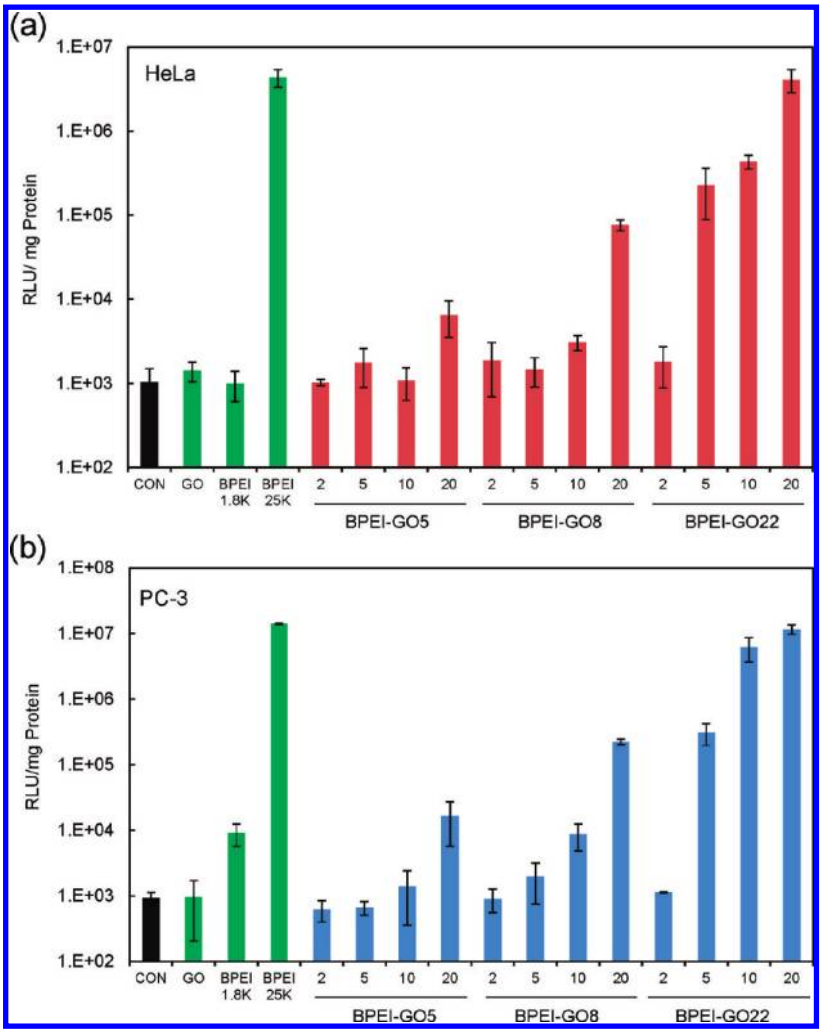

Figure 6. Transfection of GO, BPEI (1.8K and 25K), and BPEI−GO conjugates at predetermined N/P ratios in HeLa (a) and PC-3 (b) cell lines. Cells were seeded on 24-well culture plates at an initial density of 7×10^4 cells/well. The cells were incubated with the complexes in 250 μL of serum-free medium for 4 h and then incubated for 18 h in 500 μL of fresh medium containing 10% FBS. After the cells had been washed with DPBS, lysis buffer was then added in the well (200 μL/well) for lysis of cells. Luciferase reporter gene expression was evaluated using a microplate spectrofluorometer.

>10, the complexation ability of BPEI−GO5 was found to be weaker than that of unmodified BPEI, which might stem from the interfering effect of negatively charged GO through the disruption of the ionic interaction of BPEI and pDNA. The complexation ability of BPEI−GO conjugates with pDNA was enhanced with an increase in conjugation ratios because of the multivalent effect of BPEI−GO. Therefore, conjugation of positively charged BPEI to negatively charged GO ensured that BPEI−GO formed a nanosized complex with pDNA.

Along with complex formation ability, the surface charge of the nanocomplex governs the cellular uptake and transfection ability of the complex. Therefore, the surface charge of the nanocomplex was studied by ζ potential measurement (Figure 5b and Figure S2 of the Supporting Information). Over the entire range of N/P ratios, GO shows a negative ζ potential value, which clearly demonstrated its inability to form a complex with DNA. HMW BPEI25K forms a complex with pDNA at low N/P ratios and shows the highest positive value of ζ potential, while LMW BPEI1.8K has a lower ζ potential. BPEI−GO8 and BPEI−GO22 exhibited considerably higher positive ζ potentials than LMW BPEI1.8K. However, these complexes showed positive surface charges lower than that of HMW BPEI25K, and it was considered to be advantageous for BPEI−GO conjugates as the excessively high positive charge of HMW BPEI25K induced higher cytotoxicity. The positive surface charge and stable polyelectrolyte complex formation of BPEI−GO tend to interact favorably with the negatively charged cell surface, thereby facilitating efficient cellular uptake.

Gene Transfection Study. To investigate the immense potential of BPEI−GO as an efficient gene carrier, we performed the luciferase gene expression assays in HeLa and PC-3 cells. The transfection efficiency was evaluated for GO, BPEI25K, BPEI1.8K, and BPEI−GO complexes at various N/P ratios. Unmodified GO and LMW BPEI1.8K showed negligible gene transfection, but HMW BPEI25K showed stronger gene transfection ability, which is considered a gold standard in nonviral gene delivery carriers (Figure 6). Overall, the level of gene transfection was increased with an increase in the N/P ratio and conjugation ratio of BPEI to GO as shown in Figure 6. BPEI−GO22 showed considerable gene transfection even at an N/P ratio of 5. At N/P ratios of 10 and 20, transfection was comparable to that of BPEI25K in both types of cells (HeLa and PC-3). This observation of the strong gene transfection ability of BPEI−GO22 might be due to the multivalent effect of

dx.doi.org/10.1021/bc200397j | *Bioconjugate Chem.* 2011, 22, 2558−2567

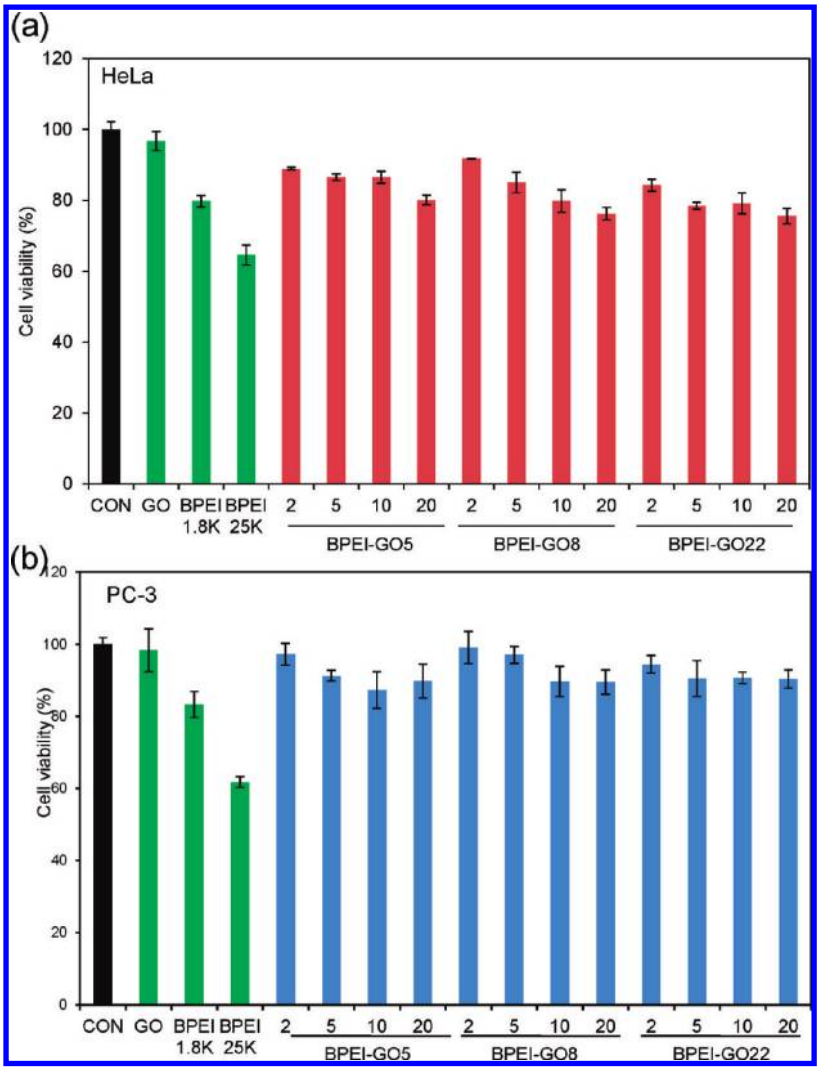

Figure 7. Cell viability profile of GO, BPEI (1.8K and 25K), and BPEI−GO conjugates at predetermined N/P ratios in HeLa (a) and PC-3 (b) cell lines. Cells were seeded onto 96-well plates at a density of 1×10^4 cells/well and incubated for 24 h. Complexes were incubated with the cells for 4 h in 100 μL of serum-free medium, followed by further incubation for 20 h in 200 μL of medium containing 10% FBS. Cell medium was replaced with 200 μL of fresh medium and 20 μL of an MTT solution (5 mg/mL) and incubated for an additional 4 h. The relative percentage of the control cells (nontreated), which were not exposed to the transfection system, was used to represent 100% cell viability.

LMW BPEI1.8K conjugated to the GO, which is favorable for formation of a stable polyelectrolyte complex with pDNA and highly positive surface charge. Though BPEI25K was considered as the gold standard in transfection, significant cytotoxicity of BPEI25K should be considered carefully before use. Therefore, the cell toxicity of all gene carriers was investigated with an MTT assay.

Cytotoxicity Assay. The cytotoxicity of GO, BPEI1.8K, BPEI25K, and BPEI−GO conjugates was studied by an MTT assay. As shown in Figure 7, GO did not show cell toxicity in HeLa cells. BPEI1.8K shows 80% cell viability; however, 40% of the cells were found to be dead in HMW BPEI25K-transfected cells. In the case of BPEI−GO, cell toxicity is increased slightly with an increase in N/P ratio, but BPEI−GO maintained >80% cell viability at all N/P ratios. Similar results were observed for PC-3 cells. Although HMW BPEI25K showed a high gene transfecion efficiency, its high cell toxicity rendered it less encouraging for practical application. However, BPEI−GO complexes demonstrated high transfection efficiency without inducing significant cytotoxicity. The low cytotoxicity of BPEI−GO can be attributed to the low cytotoxic character of LMW BPEI, which was retained in BPEI−GO even after conjugation with GO.[26−29] This implies the great potential of BPEI−GO as a nonviral gene delivery carrier with low toxicity.

Photoluminescence Study. The excellent optical property of GO makes it a very enticing agent in bioimaging and fluorescence-assisted cellular uptake tracking. In this study, we investigated the optical property of GO and BPEI−GO by UV−vis absorbance and PL spectroscopy. GO and BPEI−GO both exhibited UV−vis absorbance over a wide range of wavelengths, though the absorbance of BPEI−GO was found to be higher than that of GO (Figure 8a). The difference in absorbance could be rationalized on the basis of the accompanied surface modification during amidation and ring opening amination of epoxy moieties leading to the reduction of GO after conjugation of BPEI to GO, which is in good accordance with other reports.[37,38] The λ_{max} excitation and λ_{max} emission of BPEI-GO were found to be 480 and 520 nm, respectively (Figure 8b). Though the PL of GO and the BPEI/GO mixture was negligible, BPEI−GO displayed a significant increase in PL when excited at 480 nm; however, a further steep increase in PL intensity was observed when BPEI−GO

dx.doi.org/10.1021/bc200397j | Bioconjugate Chem. 2011, 22, 2558−2567

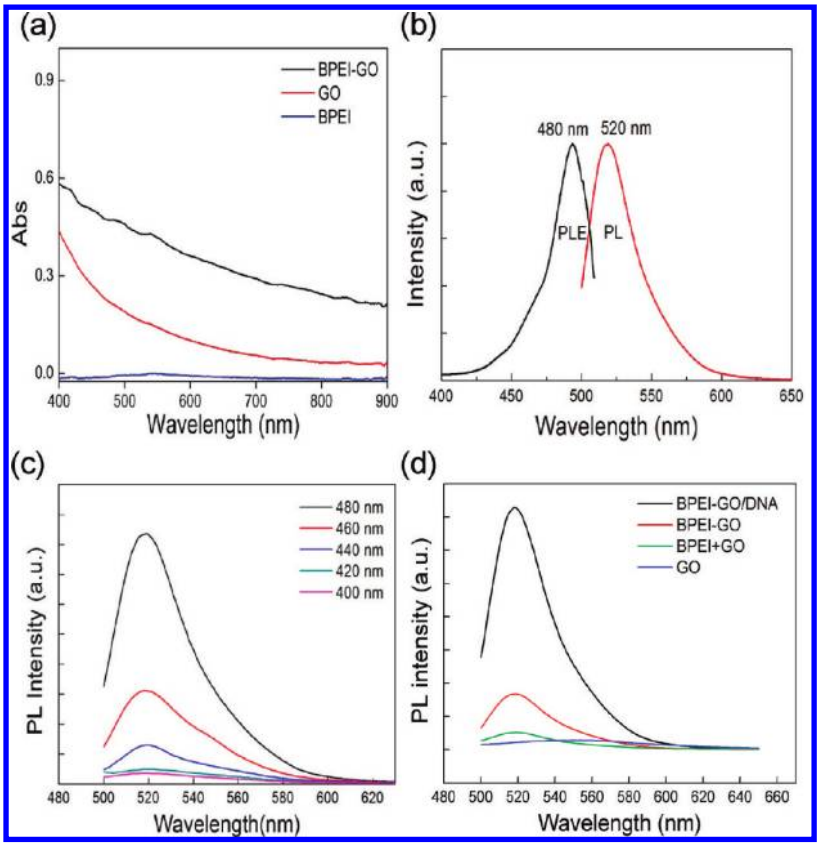

Figure 8. (a) UV−vis absorption spectrum of GO, BPEI, and BPEI−GO in water (0.01 mg/mL). (b) BPEI−GO photoluminescence excitation (PLE) spectrum with a detection wavelength of 480 nm and BPEI−GO PL spectrum excited at 480 nm. (c) BPEI−GO PL spectrum in water recorded for progressively longer excitation wavelengths from 400 to 480 nm in 20 nm increments. (d) PL spectrum of the BPEI−GO/DNA complex, BPEI−GO, the BPEI/GO mixture, and GO in water (0.01 mg/mL).

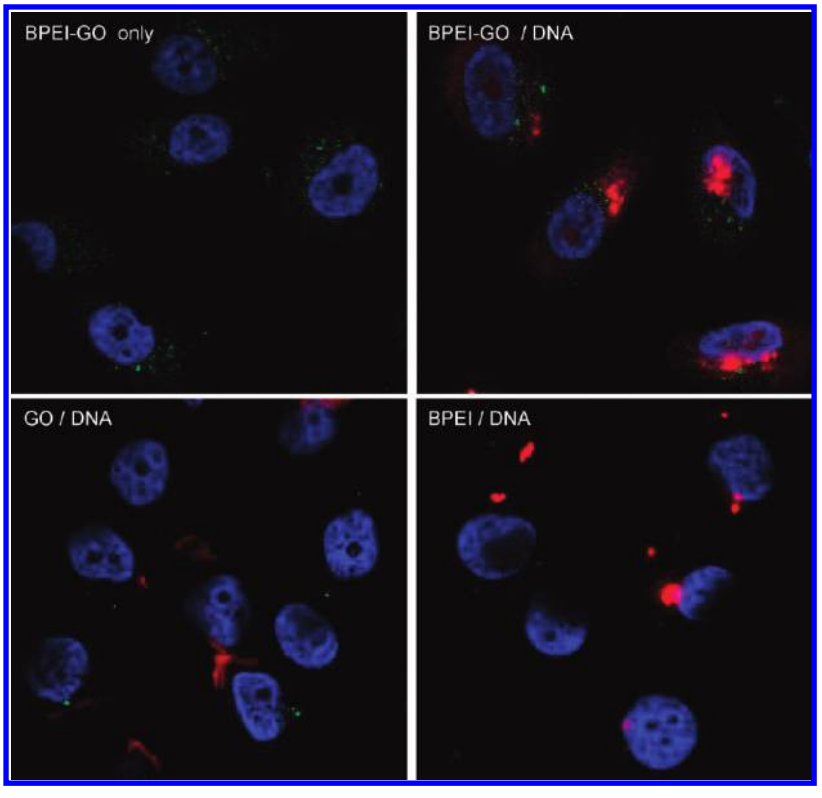

Figure 9. Confocal fluorescence microscopic images of a PC-3 cell line treated with BPEI−GO, DNA complexes with BPEI−GO, GO, and BPEI. pDNA was labeled with TOTO-3, and nuclei were stained with DAPI; a 488 nm laser was then applied to observe PL.

dx.doi.org/10.1021/bc200397j | *Bioconjugate Chem.* 2011, 22, 2558−2567

formed a complex with pDNA (Figure 8d). Both GO and BPEI−GO absorbed light over a wide range of wavelengths (Figure 8a), but GO displayed considerably low emission that could be attributed to the nonradiative emission of GO arising due to the presence of a carboxylic group and an epoxy group.[33] On the other hand, the conjugation of BPEI to GO effectively restored the conjugated aromatic clusters and suppressed the nonradiative emission of GO through nucleophilic binding of BPEI to the carboxylic group and the epoxy group of GO. At the same time, the ionic interaction between BPEI and GO adversely affected the PL; however, the combined effects gave rise to an overall increase in the PL intensity of BPEI−GO compared to that of GO. After incorporation of pDNA, BPEI preferentially formed a complex with pDNA and induced recovery of the PL intensity of BPEI−GO that was partially lost due to the ionic interaction between GO and BPEI.[39] The observed facts certainly prove the potential of BPEI-GO as a good emitter by reduction of nonradiative emission and induction of radiative emission.

Bioimaging Study. To evaluate the potential of BPEI−GO as a bioimaging reagent, we conducted the transfection studies of GO and BPEI−GO with or without pDNA complexation and tracked the movement of the complexes during the transfection using confocal microscopy (Figure 9 and Figure S3 of the Supporting Information). To visualize the movements of complexes, pDNA was labeled with TOTO-3 and nuclei were stained with DAPI, and then a 488 nm laser was applied to observe PL. No green PL was observed when GO and BPEI were employed alone, which was in accordance with a previous PL spectroscopy study. However, significant green fluorescence of BPEI−GO was observed after transfection into the cells, which confirmed the distribution of BPEI−GO in the cytosol. In addition, when the BPEI−GO/pDNA complex was transfected into cells, not only green fluorescence but also red fluorescence of pDNA was observed in cells, which demonstrated the efficacy of the developed dual-labeled complex in providing information regarding the location of BPEI−GO and pDNA. Therefore, these results clearly illustrate the potential of the BPEI−GO nanoconstruct as a bioimaging reagent.

CONCLUSION

In conclusion, to develop GO as an efficient gene carrier, it was imperative to conjugate a cationic gene carrier to GO as unlike ssDNA, dsDNA could not be loaded on GO through $\pi-\pi$ stacking interaction. Our work demonstrated the successful fabrication of GO through covalent linkage with LMW BPEI, which acted as a cationic gene carrier. It was confirmed that BPEI−GO possessed high gene delivery efficiency and exhibited high cell viability. Furthermore, the PL properties of GO were enhanced through conjugation of BPEI to GO, which advocated the immense potential of BPEI−GO as a fluorescence reagent. This highly efficient gene delivery and the excellent photoluminescence activities of the GO-based nanoconstruct will definitely merit further attention in the development of more sophisticated carrier systems that could serve both as a gene delivery vector and as a bioimaging tool. There are a few reports that demonstrated the fabrication of carbon nanotube-based nanomaterials and their enhanced efficiency in siRNA delivery[40] as well as in photothermal therapeutic applications.[41] Considering the extremely high transfection efficiency comparable to that of HMW BPEI and the high cell viability, its application could be extended to siRNA delivery, drug delivery, and photothermal therapy by installing further functional and structural attributes such as enhancing dispersibility through pegylation.

ASSOCIATED CONTENT

Supporting Information

Standard curve of BPEI quantification, ζ potentials of carriers, and confocal microscopic images of HeLa cells. This material is available free of charge via the Internet at http://pubs.acs.org.

AUTHOR INFORMATION

Corresponding Author

*Department of Chemistry, Pohang University of Science and Technology, Pohang 790-784, Korea. Phone: 82-54-279-2104. Fax: 82-54-279-3399. E-mail: wjkim@postech.ac.kr.

ACKNOWLEDGMENTS

This research was supported by the Converging Research Center Program (2011K000820) through the National Research Foundation of (NRF) funded by the Ministry of Education, Science and Technology, and a grant (K00060-283) from the Fundamental R&D Program for Core Technology of Materials funded by the Ministry of Knowledge Economy, Republic of Korea. We thank Prof. H. Choi for assistance in the AFM analysis.

REFERENCES

(1) Novoselov, K. S., Geim, A. K., Morozov, S. V., Jiang, D., Zhang, Y., Dubonos, S. V., Grigoreva, I. V., and Firsov, A. A. (2004) Electric field effect in atomically thin carbon films. *Science 306*, 666−669.

(2) Geim, A. K., and Novoselov, K. S. (2007) The rise of graphene. *Nat. Mater. 6*, 183−191.

(3) Li, X. L., Wang, X. R., Zhang, L., Lee, S. W., and Dai, H. J. (2008) Chemically derived, ultrasmooth graphene nanoribbon semiconductors. *Science 319*, 1229−1232.

(4) Yang, M., and Gong, S. (2010) Imumunosensor for the detection of cancer biomarker based on percolated graphene thin film. *Chem. Commun. 46*, 5796−5798.

(5) Hu, Y., Li, F., Bai, X., Li, D., Hua, S., Wang, K., and Niu, L. (2011) Label-free electrochemical impedance sensing DNA hybridization based on functionalized graphene sheets. *Chem. Commun. 47*, 1743−1745.

(6) Sun, X., Liu, Z., Welsher, K., Robinson, J. T., Goodwin, A., Zaric, S., and Dai, H. J. (2008) Nano-Graphene Oxide for Cellular Imaging and Drug Delivery. *Nano Res. 1*, 203−212.

(7) Peng, C., Hu, W., Zhou, W., Fan, C., and Huang, Q. (2010) Intracellular imaging with a graphene-based fluorescent probe. *Small 6*, 1686−1692.

(8) Liu, Z., Robinson, J. T., Sun, X. M., and Dai, H. J. (2008) PEGylated nanographene oxide for delivery of water-insoluble cancer drugs. *J. Am. Chem. Soc. 130*, 10876−10877.

(9) Chen, B., Liu, M., Zhang, L., Huang, J., Yao, J., and Zhang, Z. (2011) Polyethylenimine-functionalized graphene oxide as an efficient gene delivery vector. *J. Mater. Chem. 21*, 7736−7741.

(10) Yang, K., Zhang, S., Zhang, G., Sun, X., Lee, S. T., and Liu, Z. (2010) Graphene in mice: Ultrahigh in vivo tumor uptake and efficient photothermal therapy. *Nano Lett. 10*, 3318−3323.

(11) Markovic, Z. M., Harhaji-Trajkovic, L. M., Todorovic-Markovic, B. M., Kepic, D. P., Arsikin, K. M., Jovanovic, S. P., Pantovic, A. C., Dramicanin, M. D., and Trajkovic, V. S. (2011) In vitro comparison of the photothermal anticancer activity of graphene nanoparticles and carbon nanotubes. *Biomaterials 32*, 1121−1129.

(12) Zhang, Y., Tan, Y. W., Stormer, H. L., and Kim, P. (2005) Experimental observation of the quantum hall effect and Berry's phase in graphene. *Nature 438*, 201−204.

(13) Rochefort, A., and Wuest, J. D. (2009) Interaction of substituted aromatic compounds with graphene. *Langmuir 25*, 210−215.
(14) Lu, C. H., Yang, H. H., Zhu, C. L., Chen, X., and Chen, G. N. (2009) A Graphene Platform for Sensing Biomolecules. *Angew. Chem., Int. Ed. 48*, 4785−4787.
(15) Li, D., Mueller, M. B., Gilje, S., Kaner, R. B., and Wallace, G. G. (2008) Processable aqueous dispersions of graphene nanosheet. *Nat. Nanotechnol. 3*, 101−105.
(16) Lu, C. H., Zhu, C. L., Li, J., Liu, J. J., Chen, X., and Yang, H. H. (2010) Using graphene to protect DNA from cleavage during cellular delivery. *Chem Commun. 46*, 3116−3118.
(17) Tang, Z., Wu, H., Cort, J. R., Buchko, G. W., Zhang, Y., Shao, Y., Aksay, I. A., Liu, J., and Lin, Y. (2010) Constraint of DNA on functionalized graphene improves its biostability and specificity. *Small 6*, 1205−1209.
(18) Verma, I. M., and Somia, M. (1997) Gene therapy: Promises, problems and prospects. *Nature 389*, 239−242.
(19) Kim, W. J., and Kim, S. W. (2009) Efficient siRNA delivery with non-viral polymeric vehicles. *Pharm. Res. 26*, 657−666.
(20) Majeti, B. K., Karmali, P. P., Madhavendra, S. S., and Chaudhuri, A. (2005) Example of fatty acid-loaded lipoplex in enhancing in vitro gene transfer efficacies of cationic amphiphile. *Bioconjugate Chem. 16*, 676−684.
(21) Mintzer, M. A., and Simanek, E. E. (2009) Nonviral vectors for gene delivery. *Chem. Rev. 109*, 259−302.
(22) Boussif, O., Lezoualc'h, F., Zanta, M. A., Mergny, M. D., Scherman, D., Demeneix, B., and Behr, J. P. (1995) A versatile vector for gene and oligonucleotide transfer into cells in culture and in vivo: Polyethylenimine. *Proc. Natl. Acad. Sci. U.S.A. 92*, 7297−7301.
(23) Fischer, D., Bieber, T., Li, Y., Elsässer, H. P., and Kissel, T. (1999) A Novel Non-viral Vector for DNA Delivery Based on Low Molecular Weight, Branched Polyethylenimine: Effect of Molecular weight on Transfection Efficiency and Cytotoxicity. *Pharm. Res. 16*, 1273−1279.
(24) Bieber, T., and Elsässer, H. P. (2001) Preparation of a Low Molecular Weight polyethylenimine for Efficient Cell transfection. *BioTechniques 30*, 74−81.
(25) Gosselin, M. A., Guo, W., and Lee, R. J. (2001) Efficient Gene Transfer Using Reversibly Cross-Linked Low Molecular Weight Polyethylenimine. *Bioconjugate Chem. 12*, 989−994.
(26) Hu, C., Peng, Q., Chen, F., Zhong, Z., and Zhuo, R. (2010) Low Molecular Weight Polyethyleneimine Conjugated Gold Nanoparticles as Efficient Gene Vectors. *Bioconjugate Chem. 21*, 836−843.
(27) Namgung, R., Zhang, Y., Fang, Q. L., Singha, K., Lee, H. J., Kwon, I. K., Jeong, Y. Y., Park, I. K., Son, S. J., and Kim, W. J. (2010) Multifunctional silica nanotubes for dual-modality gene delivery and MR imaging. *Biomaterials 32*, 3042−3052.
(28) Namgung, R., Singha, K., Yu, M. K., Jon, S., Kim, Y. S., Ahn, Y., Park, I. K., and Kim, W. J. (2010) Hybrid superparamagnetic iron oxide nanoparticle-branched polyethylenimine magnetoplexes for gene transfection of vascular endothelial cells. *Biomaterials 31*, 4204−4213.
(29) Nunes, A., Amsharov, N., Guo, C., Van den Bossche, J., Santhosh, P., Karachalios, T. K., Nitodas, S. F., Burghard, M., Kostarelos, K., and Al-Jamal, K. T. (2010) Hybrid polymer-grafted multiwalled carbon nanotubes for in vitro gene delivery. *Small 6*, 2281−2291.
(30) Mochalin, V. N., and Gogotsi, Y. (2009) Wet chemistry route to hydrophobic blue fluorescent nanodiamond. *J. Am. Chem. Soc. 131*, 4594−4595.
(31) Liu, H., Ye, T., and Mao, C. (2007) Fluorescent carbon nanoparticles derived from candle soot. *Angew. Chem., Int. Ed. 46*, 6473−6475.
(32) Eda, G., Lin, Y. Y., Mattevi, C., Yamaguchi, H., Chen, H. A., Chen, I. S., Chen, C. W., and Chhowalla, M. (2010) Blue photoluminescence from chemically derived graphene oxide. *Adv. Mater. 22*, 505−509.
(33) Mei, Q., Zhang, K., Guan, G., Liu, B., Wang, S., and Zhang, Z. (2010) Highly efficient photoluminescent graphene oxide with tunable surface properties. *Chem. Commun. 46*, 7319−7321.
(34) Colthup, N. B., Daly, L., and Weberley, S. E. (1999) in *Introduction to Infrared and Raman Spectroscopy*, Academic Press, New York.
(35) Compton, O. C., Dikin, D. A., Putz, K. W., Brinson, L. C., and Nguyen, S. T. (2010) Electrically conductive "alkylated" graphene paper via chemical reduction of amine-functionalized graphene oxide paper. *Adv. Mater. 22*, 892−896.
(36) Dreyer, D. R., Park, S., Bielawski, C. W., and Ruoff, R. S. (2010) The chemistry of graphene oxide. *Chem. Soc. Rev. 39*, 228−240.
(37) Kim, Y. K., Kim, M. H., and Min, D. H. (2011) Biocompatible reduced graphene oxide prepared by using dextran as a multifunctional reducing agent. *Chem. Commun. 47*, 3195−3197.
(38) Zhang, Y., Chen, B., Zhang, L., Huang, J., Chen, F., Yang, Z., Yao, J., and Zhang, Z. (2011) Controlled assembly of Fe_3O_4 magnetic nanoparticles on graphene oxide. *Nanoscale 3*, 1446−1450.
(39) Nguyen, B. T., Gautrot, J. E., Ji, C., Brunner, P. L., Nguyen, M. T., and Zhu, Z. Z. (2006) Enhancing the photoluminescence intensity of conjugated polycationic polymers by using quantum dots as antiaggregation reagents. *Langmuir 22*, 4799−4803.
(40) Moon, H. K., Lee, S. H., and Choi, H. C. (2009) *In Vivo* Near-Infrared Mediated Tumor Destruction by Photothermal Effect of Carbon Nanotubes. *ACS Nano 3*, 3707−3713.
(41) Herrero, M. A., Toma, F. M., Al-Jamal, K. T., Kostarelos, K., Bianco, A., Ros, D. T., Bano, F., Casalis, L., Scoles, G., and Prato, M. (2009) Synthesis and Characterization of a Carbon Nanotube-Dendron Series for Efficient siRNA Delivery. *J. Am. Chem. Soc. 131*, 9843−9848.